A fully dispersive weakly nonlinear model for water waves

By K. Nadaoka[1], S. Beji[2] and Y. Nakagawa[3]

[1]*Graduate School of Information Science and Engineering, Tokyo Institute of Technology, 2-12-1 O-okayama, Meguro-ku, Tokyo 152, Japan*

[2]*Department of Naval Architecture and Ocean Engineering, Istanbul Technical University, Maslak 80626, Istanbul, Turkey*

[3]*Port and Harbour Research Institute, Nagase 3-1-1, Yokosuka 239, Japan*

A fully dispersive weakly nonlinear water wave model is developed via a new approach named the *multiterm-coupling technique*, in which the velocity field is represented by a few vertical-dependence functions having different wave-numbers. This expression of velocity, which is approximately irrotational for variable depth, is used to satisfy the continuity and momentum equations. The Galerkin method is invoked to obtain a solvable set of coupled equations for the horizontal velocity components and shown to provide an optimum combination of the prescribed depth-dependence functions to represent a random wave-field with diversely varying wave-numbers. The new wave equations are valid for arbitrary ratios of depth to wavelength and therefore it is possible to recover all the well-known linear and weakly nonlinear wave models as special cases. Numerical simulations are carried out to demonstrate that a wide spectrum of waves, such as random deep water waves and solitary waves over constant depth as well as nonlinear random waves over variable depth, is well reproduced at affordable computational cost.

1. Introduction

Marked by strong interactions of waves with the seabed topography as well as the foamy appearance of breaking waves, coastal zone offers vivid examples of nonlinear phenomenon. Offshore, in the open ocean, it is a rare event to observe anything but steep Stokes-type waves breaking in somewhat different fashion. Yet, while all these well-confirmed observations continue to remind us of the inadequacy of linear wave models, considerable barriers associated with nonlinearity hamper our enthusiasm greatly to use nonlinear models in practical applications. It would obviously be a desirable prospect to have a wave model that can describe the nonlinear wave evolutions at arbitrary depths at affordable computational cost by introducing plausible approximations to the formulation. This work aims precisely at achieving such a goal.

The standard way of developing a wave model is to introduce a suitable depth-dependence function, or put another way, to facilitate a depth-integration of the governing equations. By doing so, the vertical dependence is effectively removed, result-

Proc. R. Soc. Lond. A (1997) **453**, 303–319
Printed in Great Britain

ing in differential equations in the horizontal propagation directions only. A certain price must of course be paid for such convenience. For instance, a depth-integrated wave model cannot handle highly nonlinear wave motions such as overturning of the wave tip; likewise, sharp variations in bottom topography require special handling (Kirby 1986; Porter & Staziker 1995). However, for practical purposes such drawbacks do not pose major restrictions; for a sufficiently realistic wave spectrum it is acceptable to model wave transformations prior to incipient breaking, and natural seabed is usually of a gently varying form. Therefore, a depth-integrated nonlinear wave model presents itself as an attractive alternative.

The Boussinesq equations can provide quite an accurate description of nonlinear wave phenomenon in the near-shore region. The major setback of these equations is their applicable depth, which is restricted to less than a quarter of the wavelength. Although several successful attempts for extending their applicable range have been reported (see, for example, Witting 1984; Madsen *et al.* 1991; Nwogu 1993) even an improved model cannot be relied on if the depth becomes comparable with the wavelength. Equally importantly, as the nonlinear terms proportional to vertical velocity component are all neglected, the Stokes-type waves cannot be generated by any Boussinesq model.

The mild-slope equation of Berkhoff (1972) has no restriction on depth; the simulated waves may propagate at arbitrary depths with the phase and group velocities determined by the linear theory dispersion relation in its full form. However, unsteady wave evolutions or random waves cannot be described by this equation, as its applicability is limited to linear monochromatic waves with single phase-speed. The time-dependent forms of the mild-slope equation (see, for example, Smith & Sprinks 1975), on the contrary, can describe the dispersive evolution of linear random waves; but the bandwidth of the wave spectrum is required to be quite narrow. In addition to these restrictions, these equations have the drawback of not being able to simulate nonlinear effects which are known to be especially appreciable in the near-shore region.

The present work offers a generalized approach in handling both dispersivity and nonlinearity. The full-dispersivity for diversely varying wave-numbers is attained by introducing a number of depth-dependence functions (instead of a single depth-dependence function as in the formulation of the mild-slope-type equations) together with Galerkin's produce, which provides a smooth blending of discrete vertical-dependence functions to represent a broad spectrum of waves with acceptable errors. Although nonlinearity is retained to the lowest order only, the derivation of the higher-order versions is a simple task because the exact forms of the continuity and in particular the momentum equations are quite manageable, allowing straightforward extensions.

The outline of the paper is as follows. The next section states the governing equations and the boundary conditions. In § 3 the depth-integrated form of the continuity equation and an exact alternative form of the Euler equations are given. Section 4 introduces the vertical-distribution function and thus specifies the vertical dependence of the velocity field. The new wave equations are derived in § 5 and comments are made on their special cases. A detailed account of the dispersion characteristics of these equations are given in § 6. Section 7 outlines the numerical algorithm and presents sample simulations for several cases. The last section is devoted to concluding remarks.

2. Governing equations and boundary conditions

The governing equations of an incompressible inviscid homogeneous fluid are given by

$$\nabla \cdot \boldsymbol{u} + \frac{\partial w}{\partial z} = 0, \tag{2.1}$$

$$\frac{\partial \boldsymbol{u}}{\partial t} + (\boldsymbol{u} \cdot \nabla)\boldsymbol{u} + w\frac{\partial \boldsymbol{u}}{\partial z} = -\frac{1}{\rho}\nabla p, \tag{2.2}$$

$$\frac{\partial w}{\partial t} + (\boldsymbol{u} \cdot \nabla)w + w\frac{\partial w}{\partial z} = -\frac{1}{\rho}\nabla p - g, \tag{2.3}$$

$$\frac{\partial \boldsymbol{u}}{\partial z} = \nabla w, \quad \frac{\partial u}{\partial y} = \frac{\partial v}{\partial x}, \tag{2.4}$$

where $\boldsymbol{u}$, w are, respectively, the horizontal velocity vector and vertical velocity component, p the pressure and g the gravitational acceleration. A bold face symbol indicates a vector with x- and y-components only, that is, $\boldsymbol{u} = (u, v)$ and $\boldsymbol{x} = (x, y)$. The two-dimensional gradient operator, $(\partial/\partial x, \partial/\partial y)$, is denoted by ∇. The origin of the coordinate system is taken at the still water level with positive z-axis pointing upward. Equation (2.1) is the continuity equation, (2.2) and (2.3) are the Euler equations of motion, and the irrotationality conditions are stated in (2.4).

The boundary conditions for a free surface flow bounded by an impermeable rigid bottom of arbitrary shape may be stated as follows.

$$p = 0, \quad \text{at } z = \eta(\boldsymbol{x}, t), \tag{2.5}$$

$$w = \frac{\partial \eta}{\partial t} + \boldsymbol{u} \cdot \nabla \eta, \quad \text{at } z = \eta(\boldsymbol{x}, t), \tag{2.6}$$

$$\boldsymbol{u} \cdot \nabla h + w = 0, \quad \text{at } z = -h(\boldsymbol{x}), \tag{2.7}$$

in which $\eta(\boldsymbol{x}, t)$ is the free surface elevation, $h(\boldsymbol{x})$ is the local water depth as measured from the still water level. The first condition states that the pressure is zero (for convenience) at the free surface. Equation (2.6) is the kinematic free surface condition which asserts that the particles on the surface remain there. Finally, equation (2.7) is the bottom condition for a varying depth with finite slope.

3. Depth-integrated continuity and momentum equations

In its present form the continuity equation is not suitable for the development of a depth-integrated wave model. To this end we refer to the depth-integrated continuity equation which is exact:

$$\frac{\partial \eta}{\partial t} + \nabla \cdot \left(\int_{-h}^{\eta} \boldsymbol{u} \, \mathrm{d}z \right) = 0. \tag{3.1}$$

Later, in accordance with our closure relation for the velocity field we shall work with $\boldsymbol{u}$ at $z = 0$ instead of $\boldsymbol{u}$ at the actual free surface $z = \eta(\boldsymbol{x}, t)$. Invoking a Taylor series expansion of $\boldsymbol{u}$ in z, evaluating the result at $z = \eta(\boldsymbol{x}, t)$, and keeping only the lowest-order nonlinear contribution gives

$$\frac{\partial \eta}{\partial t} + \nabla \cdot \left(\int_{-h}^{0} \boldsymbol{u} \, \mathrm{d}z + \eta \boldsymbol{u}_0 \right) = 0, \tag{3.2}$$

where $\boldsymbol{u}_0$ is the horizontal velocity vector at the still water level $z = 0$. Equation (3.2) cannot be evaluated any further unless a closure relation completely defining the vertical dependence of $\boldsymbol{u}$ is invoked.

An exact momentum equation for irrotational flow can be derived from equations (2.2)–(2.5) as given in the Appendix:

$$\frac{\partial \boldsymbol{u}}{\partial t} + \nabla \left[g\eta + \int_z^\eta \frac{\partial w}{\partial t} \mathrm{d}z + \tfrac{1}{2} \left(\boldsymbol{u}_s \cdot \boldsymbol{u}_s + w_s^2 \right) \right] = 0, \tag{3.3}$$

where $\boldsymbol{u}_s$, w_s are the velocity components at the free surface $z = \eta(\boldsymbol{x}, t)$ while $\boldsymbol{u}$, w are the velocities at an arbitrary depth z, as denoted before. In the following, however, we shall use the dependent variables ($\boldsymbol{u}_0$, w_0) at the still water level $z = 0$. Employing an approach identical to that used in deriving equation (3.2), equation (3.3) becomes

$$\frac{\partial \boldsymbol{u}}{\partial t} + \nabla \left[g\eta + \int_z^0 \frac{\partial w}{\partial t} \mathrm{d}z + \eta \frac{\partial w_0}{\partial t} + \tfrac{1}{2} \left(\boldsymbol{u}_0 \cdot \boldsymbol{u}_0 + w_0^2 \right) \right] = 0, \tag{3.4}$$

in which $\boldsymbol{u}_0$, w_0 are the velocities at the still water level $z = 0$. Since only the lowest-order nonlinear terms are retained, equations (3.2) and (3.4) are correct to $O(\varepsilon^2)$ in nonlinearity. As there is no restriction on the applicable depth of equations (3.2) and (3.4) the nonlinearity parameter ε may be considered as ka or a/h (a and k are respectively typical wave amplitude and wave-number), depending on the non-dimensionalization procedure adopted. An alternative is to use the parameter ga/C_p^2 with C_p denoting the wave phase velocity (Beji 1995). This unified definition includes ka and a/h as its special cases and avoids problems associated with the domains of validity.

4. A closure relation

Mathematical procedure of obtaining a water-wave equation is in general a conversion process from the governing equations defined in three-dimensional (x, y, z) space to the wave equations to be defined in horizontal two-dimensional (x, y) space. For this conversion, as indicated before, it is necessary to specify the vertical dependence of the velocity field. In principle, any specification which fulfils the bottom and irrotationality conditions is permissible; of course the quality of the solution is directly dependent on the form adopted. For instance, the Boussinesq equations are obtained by introducing an asymptotic expansion of the velocity potential around the long wave limit, in which the vertical dependence of the velocity field is represented by polynomials in z. Such an asymptotic expansion necessarily restricts the applicable depth of the resulting equations by the terms retained, which, for practical reasons, cannot be many. Obviously, a wave model without depth restriction cannot be constructed in this manner and a more general approach to represent the vertical distribution of the potential field must be introduced.

A natural choice for the vertical-dependence function follows from the general solution of Laplace's equation for horizontal bottom:

$$\Phi(x, z, t) = \int_{-\infty}^{+\infty} A(k, t) \frac{\cosh k(h + z)}{\cosh kh} \exp(\mathrm{i}kx) \, \mathrm{d}k, \tag{4.1}$$

where k is the wave-number, $\Phi(x, z, t)$ is the two-dimensional potential function and $A(k, t)$ is the wave-number spectrum of this particular potential. Equation (4.1) is

exact only when both k and h are independent of the spatial coordinates; for variable depth the exact solution of Laplace's equation is quite complicated (see, for instance, Miles 1985). Nevertheless, if the depth varies *slowly* it is plausible to expect that (4.1) is still a good approximation with k and h referring to their local values, as in the mild-slope equation (Mei 1983, p. 87). In the following we shall adopt this line of approach to keep the final equations as simple as possible. The precise meaning of this approximation is clarified at the end of this section. It should also be noted that the general solution (4.1) is subject only to the bottom boundary condition and its applicability is not necessarily restricted to linear waves as the linearity or nonlinearity of the wave model is dictated by the free-surface boundary conditions.

In this work, as it is evident from (3.2) and (3.4), a perturbation approach is adopted by using the velocity components at the still water level $(\boldsymbol{u}_0, w_0)$ and retaining only the lowest-order nonlinear terms. This is an acceptable truncation so long as the deep water nonlinear resonant interactions (Phillips 1960) are neglected. However, inclusion of the higher-order contributions is straightforward and can be accomplished in the same manner; such a model would be desirable for the simulation of nonlinear wave modulations on deep water.

Considering equation (4.1), the horizontal velocity vector is expressed as a sum, each term comprising a vertical-dependence function $F_m(z, k_m h)$ and a corresponding velocity vector at the still water level $\boldsymbol{U}_m(\boldsymbol{x}, t)$ which is independent of z:

$$\boldsymbol{u}(\boldsymbol{x}, z, t) = \sum_{m=1}^{N} F_m(z, k_m h)\boldsymbol{U}_m(\boldsymbol{x}, t), \quad F_m(z, k_m h) = \frac{\cosh k_m(h+z)}{\cosh k_m h}, \tag{4.2}$$

where $\boldsymbol{U}_m(\boldsymbol{x}, t)$ is the mth component of the horizontal velocity vector at the still water level and $k_m = \mid \boldsymbol{k}_m \mid$. Note the resultant horizontal velocity vector at $z = 0$ is the sum of the depth-independent velocity components: $\boldsymbol{u}_0 = \sum \boldsymbol{U}_m$.

Unlike the discrete version of (4.1) (i.e. the integral replaced with a summation over different wave-numbers) equation (4.2) does not impose any definite horizontal dependency on the velocity components and therefore provides greater freedom for the representation of the velocity field. Naturally, this enhanced freedom requires the additional work of determining different $\boldsymbol{U}_m(\boldsymbol{x}, t)$, which is accomplished here by the Galerkin procedure. In contrast to the spectral methods based on the discrete form of (4.1) (see, for instance, Fenton & Rienecker 1980), the Galerkin method leads to couplings among different velocity components even for linear waves and hence endows the wave model with the capability to propagate broad-banded wave fields by retaining only a few terms in (4.2), as is demonstrated in § 7 (*a*). Such an approach of representing the dynamics of a broad-banded wave field may be termed as the *multiterm-coupling technique*. Since the accurate representation of the velocity profile leads to better dispersion characteristics, it is sufficient to take only a few terms in (4.2) for excellent linear dispersion characteristics over a wide frequency band. Nonlinear dispersion characteristics on the other hand are dictated by the perturbation terms retained in (3.2) and (3.4) and these terms enable the resulting wave model to accommodate amplitude-dispersion.

The vertical velocity is obtained from equation (2.1) by substituting (4.2) and then integrating from bottom to an arbitrary depth z:

$$w(\boldsymbol{x}, z, t) = -\sum_{m=1}^{N} \nabla \cdot \left[\frac{\sinh k_m(h+z)}{k_m \cosh k_m h}\boldsymbol{U}_m(\boldsymbol{x}, t)\right]. \tag{4.3}$$

It is worthwhile to point out that, when both k and h are taken to be spatially varying quantities, $w(\boldsymbol{x}, z, t)$ satisfies the bottom condition, equation (2.7), *exactly* for the horizontal velocity specified in (4.2). Clearly, this advantage has been purchased at the expense of the irrotationality condition, which now reads $\boldsymbol{u}_z - \nabla w = O[\nabla(k_m h)(\nabla \cdot \boldsymbol{U}_m)]$. The approximate character of the present formulation for variable depth originates from this small but non-zero rotationality. Nevertheless, as the demonstrated success of the mild-slope-type equations for variable bathymetry justifies such an approximation, it is adopted here as well, in order that refraction effects can properly be accounted for.

5. Fully dispersive weakly nonlinear wave equations

Having established the depth-dependence of velocity field by (4.2), the continuity equation (3.2) may now be evaluated:

$$\frac{\partial \eta}{\partial t} + \sum_{m=1}^{N} \nabla \cdot \left[\left(\frac{\omega_m^2}{g k_m^2} + \eta \right) \boldsymbol{U}_m \right] = 0, \tag{5.1}$$

where use has been made of the linear dispersion relation $\omega_m^2 = g k_m \tanh k_m h$ for notational convenience. Its appearance is a natural consequence of the assumption made about the vertical dependence of the velocity field. Equation (5.1) is correct to $O(\varepsilon^2)$ in nonlinearity and incorporates the effect of varying depth through k_m, which is in general not constant.

If there were a single $\boldsymbol{U}$ as in the Boussinesq formulation, a simple substitution of (4.2) and (4.3) into (3.4) would be sufficient to obtain the momentum equation necessary to solve for $\boldsymbol{U}$. In this case however there are N number of unknown velocity vectors ($\boldsymbol{U}_m, m = 1, \ldots, N$) which in turn necessitate N momentum equations corresponding to each $\boldsymbol{U}_m$. In such a case the Galerkin weak formulation, a procedure distinguished by its close correspondence with variational formulations, offers a well-established and straightforward approach. According to this method, after substituting (4.2) and (4.3) into (3.4), the resulting equation is multiplied by the depth-dependence function, $F_n(z, k_n h)$, and integrated over the depth. Since the depth-dependence function has N different modes, one obtains a total of N vector equations corresponding to each mode. These equations together with the continuity equation, (5.1), constitute a system of $2N+1$ number of coupled nonlinear differential equations which can be used for obtaining $2N + 1$ unknowns ($\eta, \boldsymbol{U}_m(u_m, v_m), m = 1, \ldots, N$) hence the complete solution to the problem posed. If the procedure is carried out

$$\begin{aligned} \int_{-h}^{0} F_n \Bigg\{ \sum_{m=1}^{N} F_m \frac{\partial \boldsymbol{U}_m}{\partial t} + \nabla \left[g\eta + \eta \frac{\partial w_0}{\partial t} + \tfrac{1}{2}(\boldsymbol{u}_0 \cdot \boldsymbol{u}_0 + w_0^2) \right] \Bigg\} \mathrm{d}z \\ = \frac{\partial}{\partial t} \int_{-h}^{0} F_n \Bigg\{ \sum_{m=1}^{N} \frac{(1 - F_m)}{k_m^2} \nabla(\nabla \cdot \boldsymbol{U}_m) + 2 \sum_{m=1}^{N} \nabla \left[\frac{(1 - F_m)}{k_m^2} \right] (\nabla \cdot \boldsymbol{U}_m) \Bigg\} \mathrm{d}z \end{aligned} \tag{5.2}$$

where $\boldsymbol{u}_0 = \sum \boldsymbol{U}_m$ as indicated before. The vertical component of the surface velocity w_0 may be obtained from (4.3) by setting $z = 0$ or from the kinematic free surface condition.

Evaluating the integrals in (5.2) the final form of the momentum equation is

obtained as

$$\sum_{m=1}^{N} A_{nm}\frac{\partial \boldsymbol{U}_m}{\partial t} + B_n\nabla\left[g\eta + \eta\frac{\partial w_0}{\partial t} + \tfrac{1}{2}\left(\boldsymbol{u}_0\cdot\boldsymbol{u}_0 + w_0^2\right)\right] = \frac{\partial}{\partial t}\sum_{m=1}^{N}\left[C_{nm}\nabla(\nabla\cdot\boldsymbol{U}_m) + \boldsymbol{D}_{nm}(\nabla\cdot\boldsymbol{U}_m)\right], \tag{5.3}$$

where

$$\left.\begin{aligned} &A_{nm} = \frac{\omega_n^2-\omega_m^2}{k_n^2-k_m^2}, \quad A_{nn} = \frac{g\omega_n^2 + h(g^2k_n^2-\omega_n^4)}{2gk_n^2},\\ &B_n = \omega_n^2/k_n^2, \quad C_{nm} = (B_n - A_{nm})/k_m^2, \quad \boldsymbol{D}_{nn} = \nabla C_{nn},\\ &\boldsymbol{D}_{nm} = \frac{4}{(k_m^2-k_n^2)}\frac{\nabla k_m}{k_m}\left[A_{nm} - (k_m^2-k_n^2)C_{nm}\right]\\ &\qquad + \frac{4}{(k_m^2-k_n^2)}\frac{\nabla h}{h}[(A_{nn}-\tfrac{1}{2}B_n)(A_{mm}-\tfrac{1}{2}B_m)]^{1/2} \end{aligned}\right\}, \tag{5.4}$$

in which the cyclic wave frequencies and corresponding wave-numbers are related by the linear theory dispersion relation as in (5.1). The free index n runs from 1 to N, resulting in N momentum equations for the component vectors $\boldsymbol{U}_m$ $(m = 1, \ldots, N)$. Thus, equations (5.1) and (5.3) constitute a solvable set of coupled equations to describe the evolutions of a fully dispersive weakly nonlinear wave field. The full-dispersivity for a broad-banded wave field can be attained by taking only a few terms, $N = 2$ or 3, as demonstrated in the following section.

An important special case is the single-component (i.e. a single-term representation of $\boldsymbol{u}$ and w: $N = 1$) forms of (5.1) and (5.3), which are:

$$\frac{\partial\eta}{\partial t} + \nabla\cdot\left[\left(\frac{C_p^2}{g} + \eta\right)\boldsymbol{u}_0\right] = 0, \tag{5.5}$$

$$C_pC_g\frac{\partial\boldsymbol{u}_0}{\partial t} + C_p^2\nabla\left[g\eta + \eta\frac{\partial w_0}{\partial t} + \tfrac{1}{2}\left(\boldsymbol{u}_0\cdot\boldsymbol{u}_0 + w_0^2\right)\right] = \frac{\partial}{\partial t}\left\{\frac{C_p(C_p-C_g)}{k^2}\nabla(\nabla\cdot\boldsymbol{u}_0) + \nabla\left[\frac{C_p(C_p-C_g)}{k^2}\right](\nabla\cdot\boldsymbol{u}_0)\right\}, \tag{5.6}$$

where $\boldsymbol{u}_0 = \boldsymbol{U}_1$ is the horizontal velocity vector at $z = 0$. C_p, C_g and k denote respectively the phase and group velocities and wave-number, computed according to the linear theory for a prescribed dominant frequency ω and a local depth h. Equations (5.5) and (5.6) may be considered as a model for narrow-banded weakly nonlinear wave field propagating over varying depth. In the non-dispersive limit when $C_p \simeq C_g \simeq (gh)^{1/2}$ the equations reduce to Airy's shallow water equations. If, instead of using the exact expressions, C_p and C_g are approximated to the second-order as $(gh)^{1/2}(1 - k^2h^2/6)$ and $(gh)^{1/2}(1 - k^2h^2/2)$ respectively then a straightforward manipulation yields the Boussinesq equations. Furthermore, (5.5) and (5.6) may be combined to obtain a single nonlinear wave equation for the surface displacement; the linearized form of the combined equation gives a new version of the time-dependent mild-slope equation (Beji & Nadaoka 1997). The removal of the harmonic time-dependency leads to Berkhoff's (1972) mild-slope equation, which in turn contains the Helmholtz equation and Lamb's shallow water equation as special cases.

6. Dispersion characteristics of new wave equations

While the Galerkin weak formulation may be regarded as a solvability condition imposed upon the momentum equation, its additional function of enhancing the dispersion characteristics of the resulting wave model should also be appreciated. Simply stated, this procedure establishes an optimum combination of the prescribed depth-dependence functions to represent a profile which does not necessarily correspond to any one of the selected depth-dependence functions. Therefore, the prescribed wave-numbers need neither cover all the wave-numbers present in a given sea state nor correspond to harmonic frequencies. In general, judiciously chosen one component (i.e. a single-term representation of $\boldsymbol{u}$ and w) is sufficient to represent a narrow-banded sea state accurately; for a broad-banded spectrum two or three components are enough. The preceding argument is rather abstract and must be exemplified to provide palpable evidence. Suppose that three vertical-dependence functions with wave-numbers k_1, k_2 and k_3 are chosen to represent a velocity profile with an arbitrary wave-number k_a. In mathematical terms we have

$$F_a(z, k_a h) = \alpha_1 F_1(z, k_1 h) + \alpha_2 F_2(z, k_2 h) + \alpha_3 F_3(z, k_3 h), \tag{6.1}$$

where $F_m(z, k_m h)$ is as defined in (4.2) and α_1, α_2, α_3 are unknown coefficients to be determined. According to Galerkin's method, (6.1) is multiplied by each one of the trial functions $F_1(z, k_1 h)$, $F_2(z, k_2 h)$, $F_3(z, k_3 h)$ in turn and integrated over the domain of interest $(-h, 0)$ to obtain a set of linear algebraic equations for the unknown coefficients α_1, α_2, and α_3. Figure 1 illustrates the performance of the approximate solutions obtained by using the trial functions $F_1(z, k_1 h)$, $F_2(z, k_2 h)$, $F_3(z, k_3 h)$ with $k_1 h = \pi/4$, $k_2 h = \pi$, $k_3 h = 3\pi$. Here, the precise values of $k_m h$'s are not crucial as long as they are properly distributed over the range of interest. The solid lines show the depth profiles to be represented (corresponding to the desired k_a as computed from the left-hand side of (6.1)) while the circles denote the computational results (obtained from the right-hand side of (6.1)). Note that even the extreme cases of $k_a h = 0$ and $k_a h = 500\pi$ are well approximated. The fact that $F_a(z, k_a h)$ for *arbitrary* $k_a h$ can be well approximated by only three $F_m(z, k_m h)$'s with *fixed* $k_m h$'s verifies the previously stated point that taking only a few terms in (4.2) is sufficient for representing a random wave-field composed of a wide range of wave-numbers.

For a clearer picture we shall now examine the single and multi-component forms of the linear dispersion relations as obtained from the new wave equations. Let us first consider the dispersion relation of a unidirectional single-component model as obtained from the linearized forms of (5.5) and (5.6) by substituting $\eta = a \exp[\mathrm{i}k_a(x - C_a t)]$, $u_0 = b \exp[\mathrm{i}k_a(x - C_a t)]$ and solving an eigenvalue problem (see, for instance, Mei 1983, p. 510):

$$C_a^2 = C_p^3 \left[C_g + \frac{k_a^2}{k^2}(C_p - C_g) \right]^{-1} \tag{6.2}$$

where k_a denotes an arbitrary incident wave-number which is free to take on any value between *zero* and *infinity*. C_a is the phase celerity dictated by the dispersion relation (6.2) for this particular wave-number k_a. C_p and C_g are the phase and group velocities corresponding to the prescribed (fixed) wave-number k ($= k_1$ or k_2 or k_3). Figure 2*a* depicts the dispersion curves for three different cases of k as computed from (6.2) against the exact expression of linear theory $(C_a)_e = (g/k_a \tanh k_a h)^{1/2}$. The water depth h was set to unity. As is seen, each selected component produces a

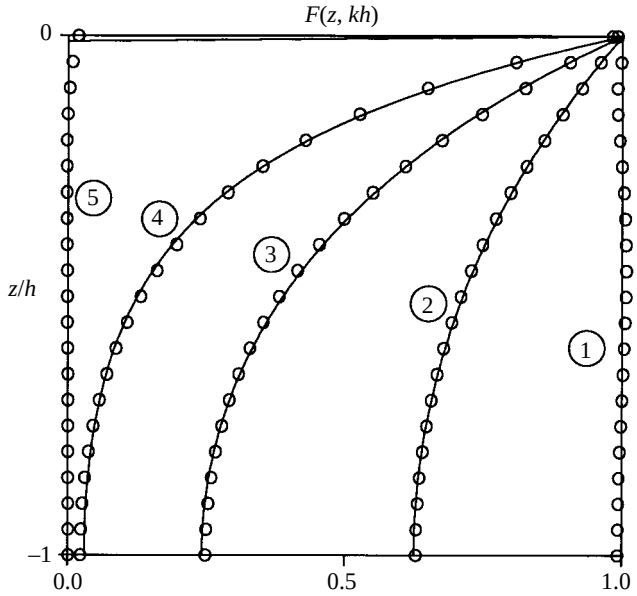

Figure 1. Comparisons of the exact and approximate vertical distribution functions for ①: $k_a h = 0$, ②: $k_a h = \frac{1}{3}\pi$, ③: $k_a h = \frac{2}{3}\pi$, ④: $k_a h = \frac{4}{3}\pi$, ⑤: $k_a h = 500\pi$. Solid lines are the exact profiles and circles denote the approximate solutions obtained via Galerkin's method using three depth-dependence functions with $k_1 h = \frac{1}{4}\pi$, $k_2 h = \pi$ and $k_3 h = 3\pi$.

dispersion curve which is tangent to the exact curve at the prescribed wave-number k. Obviously, the applicable domain of the single-component model is not confined to the selected wave-number itself but, with acceptable errors, to a narrow-band of wave-numbers centred around that particular wave-number.

The dispersion relation of the multi-component equations with three prescribed wave-numbers ($k_1 h = \frac{1}{4}\pi$, $k_2 h = \pi$, $k_3 h = 3\pi$) can be obtained by considering the linearized versions of (5.1) and (5.3) for $N = 3$. The procedure is in exactly the same line with that of the single component but longer; therefore no detail is given here. Figure 2*b* compares the exact dispersion relation of linear theory with the relation obtained from the eigenvalue solution of the wave equations with three components. The agreement is virtually perfect for the range considered, which covers a very broad-band wave-number spectrum, indicating that overall the Galerkin procedure provides quite acceptable approximations.

A question of importance is the number of components to be included for an acceptable representation of a given sea state. As shown above, taking three velocity components is quite satisfactory for relatively broad-banded wave fields. Increasing the number of components usually brings only marginal improvements which are not justified against the increased computation time. Using only two components on the other hand causes a filtering effect since the propagation of certain frequency components is hindered. If the single-component model is used to represent a broad-banded spectrum the computed wave profiles look smoothed in comparison with the actual waves as higher frequency wave contributions are not properly accounted for. Of course, for monochromatic, bichromatic or narrow-banded irregular waves, use of the single-component model is amply justified and increasing the number of components brings no detectable improvement at all.

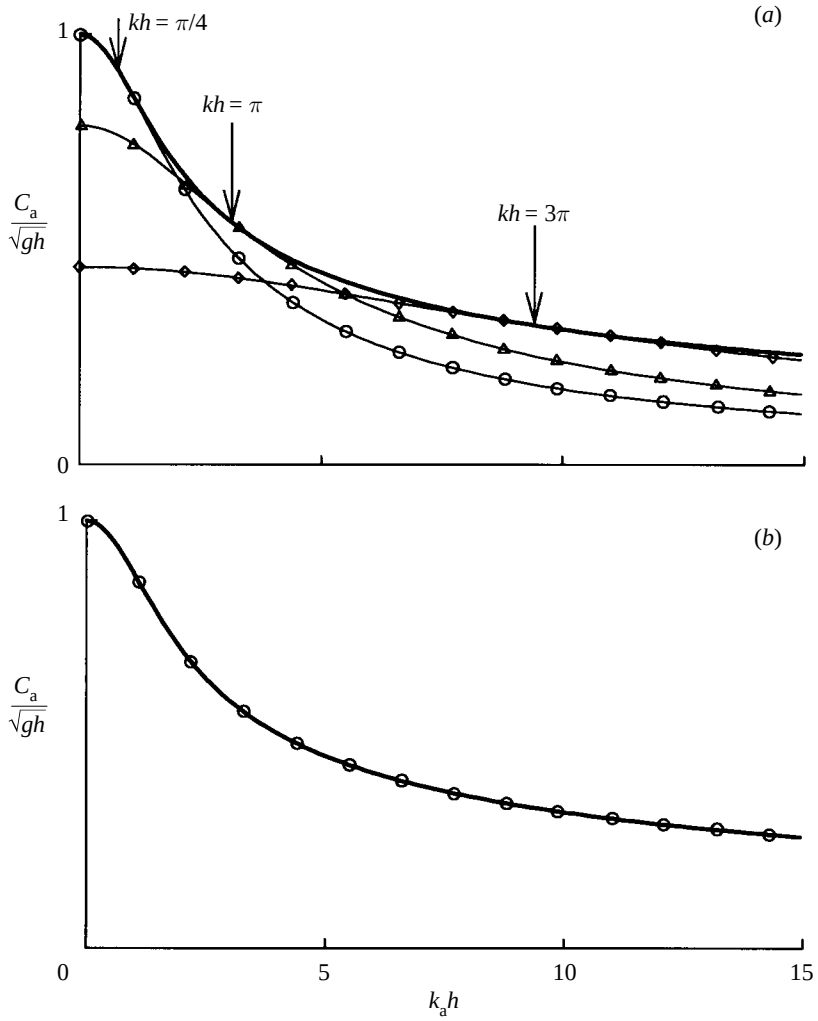

Figure 2. (*a*) Linear theory dispersion relation (—) and dispersion relations of the single-component wave model for three different cases: $kh = \pi/4$ (○), $kh = \pi$ (△) and $kh = 3\pi$ (◇). (*b*) Linear theory dispersion relation (—) and dispersion relation of the three-component wave model (○) constructed from three different depth-dependence functions with $k_1h = \frac{1}{4}\pi$, $k_2h = \pi$, $k_3h = 3\pi$.

7. Numerical tests for one-dimensional waves

The general forms of the wave equations, (5.1) and (5.3), are in perfect correspondence with those of the Boussinesq equations. From the computational point of view this is an important advantage because it allows the adoption of an implicit scheme which leads essentially to a tridiagonal matrix that can be solved quite efficiently. The main difference between the wave equations derived here and the Boussinesq equations is in the number of equations involved. Considering the one-dimensional case for instance, there are N momentum equations (N is usually no more than 3) instead of one momentum equation of the Boussinesq theory. This naturally brings an increase to the computational time when compared with the Boussinesq models but not a drastic one; especially if a generalized Thomas algorithm, or the so-called

the block elimination method is used (see Keller 1974). In the present numerical routine this method was used for solving the linear algebraic equations resulting from implicit, three-time-level, centred discretizations of the momentum equations:

$$\sum_{m=1}^{N}\left[\left(\frac{C_{nm}}{\Delta x^2}-\frac{D_{nm}}{2\Delta x}\right)u_{m,i-1}^{k+1}-\left(A_{nm}+2\frac{C_{nm}}{\Delta x^2}\right)u_{m,i}^{k+1}+\left(\frac{C_{nm}}{\Delta x^2}+\frac{D_{nm}}{2\Delta x}\right)u_{m,i+1}^{k+1}\right]$$
$$=\sum_{m=1}^{N}\left[\left(\frac{C_{nm}}{\Delta x^2}-\frac{D_{nm}}{2\Delta x}\right)u_{m,i-1}^{k-1}-\left(A_{nm}+2\frac{C_{nm}}{\Delta x^2}\right)u_{m,i}^{k-1}+\left(\frac{C_{nm}}{\Delta x^2}+\frac{D_{nm}}{2\Delta x}\right)u_{m,i+1}^{k-1}\right]$$
$$+\frac{\Delta t}{\Delta x}B_n\left\{g(\eta_{i+1}^k-\eta_{i-1}^k)+\tfrac{1}{2}\left[(u_{0,i+1}^k)^2-(u_{0,i-1}^k)^2+(w_{0,i+1}^k)^2-(w_{0,i-1}^k)^2\right]\right\}$$
$$+\frac{1}{2}\frac{B_n}{\Delta x}\left[\eta_{i+1}^k(w_{0,i+1}^{k+1}-w_{0,i+1}^{k-1})-\eta_{i-1}^k(w_{0,i-1}^{k+1}-w_{0,i-1}^{k-1})\right], \tag{7.1}$$

where the superscripts and subscripts stand respectively for the time levels and spatial nodes while Δt and Δx denote the corresponding increments in time and space. The new time level values of the velocities components, $u_{m,i}^{k+1}$, are the only unknowns to be solved at each time step. The resulting matrix equation is block tridiagonal and can be solved very efficiently by taking advantage of the generalized version of the Thomas algorithm, as indicated before.

The corresponding discretization of the continuity equation results in an explicit form which requires no special solution technique:

$$\eta_i^{k+1}=\eta_i^{k-1}-\frac{\Delta t}{\Delta x}\sum_{m=1}^{N}\left[\left(\frac{\omega_m^2}{gk_{m,i+1}^2}+\eta_{i+1}^k\right)u_{m,i+1}^k-\left(\frac{\omega_m^2}{gk_{m,i-1}^2}+\eta_{i-1}^k\right)u_{m,i-1}^k\right], \tag{7.2}$$

in which η_i^{k+1} is the only unknown. The first two time level values of the surface displacement and velocity components are specified according to the prescribed initial conditions, which are usually taken to be zero throughout the computational domain, representing the state of rest. It is of course possible to commence a computation from a different initial configuration, such as a given free surface displacement and velocity field. The incident waves are introduced at the incoming boundary by specifying the surface displacement and the corresponding surface velocity at each time step.

The coefficients in equation (5.4) are determined by first selecting definite frequencies and then computing the related wave-numbers for the given local depth according to the linear theory dispersion relation. For computational robustness it has been found necessary to express the nonlinear terms w_0^2 and $(\eta w_0^2)_t$ in terms of the horizontal velocity components using the linearized kinematic free surface condition and the linearized continuity equation.

Three cases are presented below as demonstrative simulations: random deep water waves, solitary waves, and nonlinear waves over variable topography. The model can simulate the other well-known wave forms (e.g., cnoidal and Stokes second-order waves); however, they are omitted here for the sake of briefness and considered in the accompanying work (Beji & Nadaoka 1997).

(*a*) *Random deep water waves*

In order to demonstrate the capability of the new wave equations to represent a broad-banded wave field with as few as three components ($N = 3$) the simulation

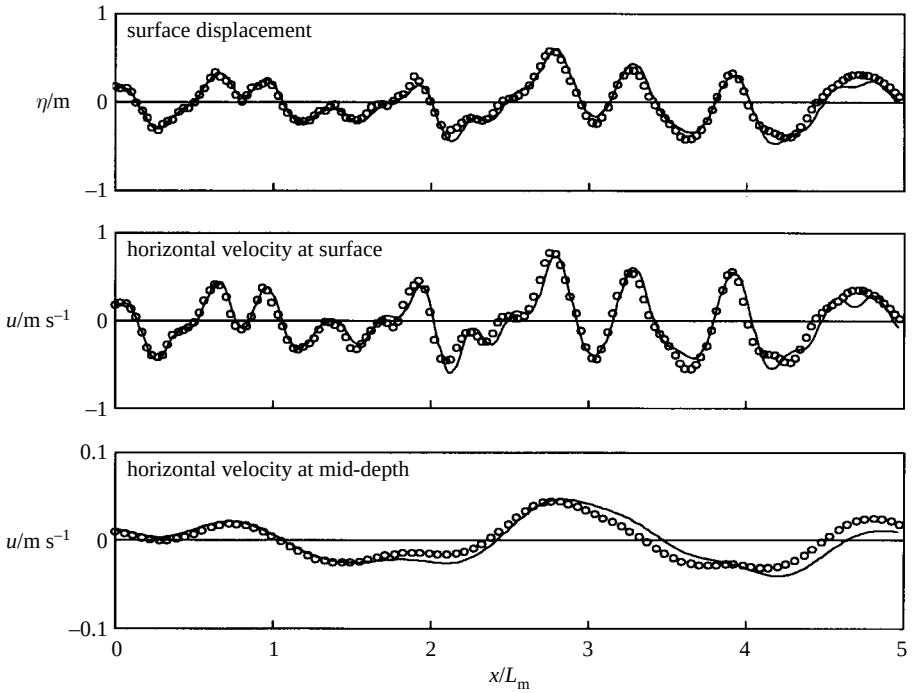

Figure 3. Deep-water random wave simulations: linear superposition of 150 sinusoidal waves with differing frequencies and phases (—) versus numerical solution of the linearized three-component wave equations (○) comprising three depth-dependence functions with $k_1h = 2\pi$, $k_2h = 3\pi$, $k_3h = 5\pi$.

of linear random waves on deep water is considered first. The depth to the mean-wavelength (denoted as L_m and defined as the average of the wavelengths in a given record) ratio is one, $h/L_m = 1$, and the time series is produced by superimposing 150 sinusoidal waves with different frequencies and random phases to generate a Bretschneider-type broad-banded spectrum. In the computation the following wave numbers were used: $k_1h = 2\pi$, $k_2h = 3\pi$, $k_3h = 5\pi$. Through numerical experiments it has been confirmed that as long as the k_mh (or rather the ω_m) were specified to cover the spectral range of the incident wave field the computational results showed negligibly small difference for different sets of k_mh. Figure 3 compares the simulations with the generated surface displacement and horizontal velocity at two different depths after 20 wave periods elapsed over a distance of five wavelengths. For only three components the performance of the wave model is remarkably good, not only in simulating the surface deformations but also the velocity field. The selection of the number of components was based on a compromise between accuracy and computational time. No sponge layer was needed to improve the absorption at the outgoing boundary; the computational domain was not longer than shown. Good absorption of the waves is attributed to the fact that the outgoing waves are radiated at three different wave-numbers instead of one. This is an important advantage especially in long time simulation of random waves.

(*b*) *Solitary wave*

The solitary wave represents the balance between nonlinearity and dispersion. Because of both theoretical and practical reasons the literature about the solitary wave

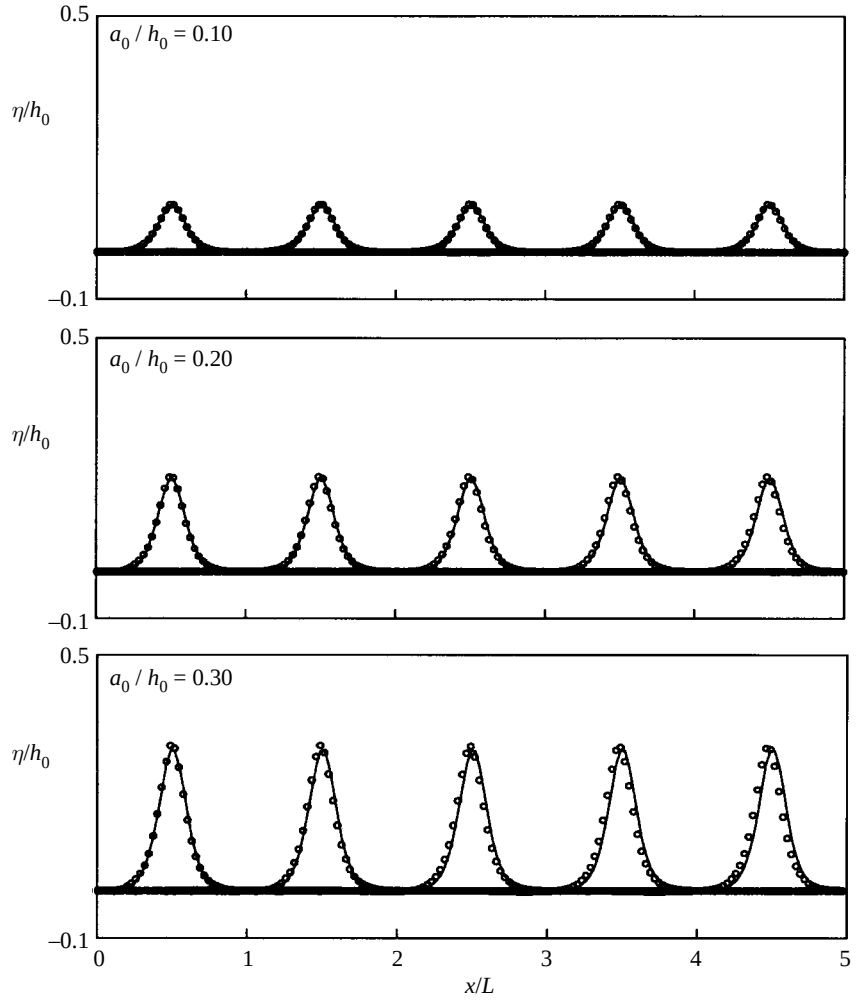

Figure 4. Analytical expression of solitary wave (—), $a \cdot \cosh^{-2}[(3a/4h^3)^{1/2}(x - ct)]$, compared with numerical solution of the present wave equations (∘) for $N = 1$ component. The phase celerity of the analytical wave is taken as $[g(h + a)]^{1/2}$ with h and a denoting respectively to the water depth and wave amplitude. The water depth is 1 m and the time intervals between the wave crests are 9, 6, and 5 s, respectively, from top to bottom.

is immense, and any nonlinear wave model that is claimed to be applicable in shallow water must be able to simulate this particular wave with acceptable accuracy. In theory it is not possible to define a finite period and wavelength for the solitary wave but for practical purposes plausible approximations can be made to specify a non-zero wave-number and frequency. In the computations h/L was taken as $1/50$ so that for a given depth a definite wavelength satisfying the long-wave condition could be obtained. The wave frequency was then determined from the linear theory dispersion relation, in compliance with the formulation of the present wave equations. Numerous tests showed that the computational results were quite insensitive to the prescribed h/L ratio as long as $h/L < 1/50$. Figure 4 depicts the numerical results and the analytical solutions for three different amplitude to depth ratios. The wavelength unit for the horizontal axis was taken as the distance between the points

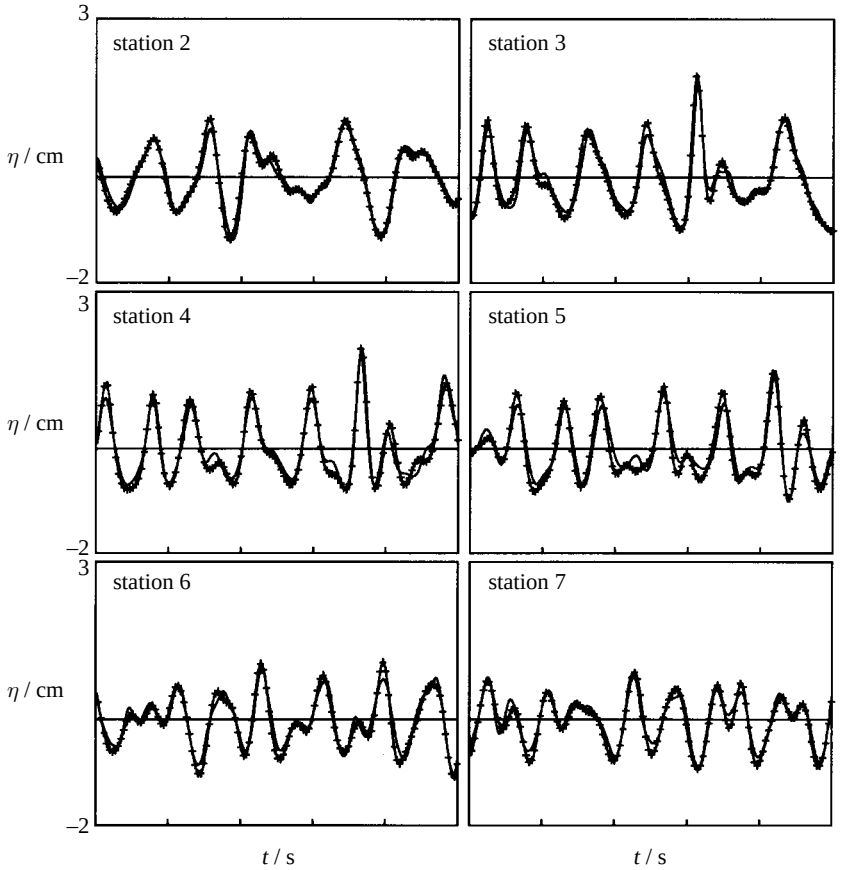

Figure 5. Comparisons of the experimental measurements of nonlinear random wave propagation over a submerged bar (—) with the numerical simulations (+) using the new wave model with two components $N = 2$. Station 2: upslope 1:20, water depth 0.16 m; station 3 and 4: horizontal bottom, water depth 0.1 m; station 5: downslope 1:10, water depth 0.18 m; station 6: downslope 1:10, water depth 0.3 m; station 7: horizontal bottom, water depth: 0.4 m.

at which the surface elevation was above 0.1% of the amplitude. As is seen from the figure, except for small phase discrepancies, the simulations are quite satisfying.

(*c*) *Nonlinear random waves*

The last case aims at testing both linear/nonlinear dispersion and shoaling characteristics of the multi-component nonlinear model for random waves. The comparisons in figure 5 for six different stations are with the experimental measurements of Beji & Battjes (1994) for nonlinear random waves travelling over a submerged trapezoidal bar. The water depth in the deeper part of the wave flume is 0.4 m and following a 1:20 upslope it reduces to a constant depth of 0.1 m. This shallow depth region continues for 2 m and then a 1:10 downslope section follows, causing the water depth to increase back to 0.4 m (see figure 1 in Beji & Battjes 1994). The incident wave field has a JONSWAP type random wave spectrum with $h/L_p = 0.1$ where L_p is the wavelength corresponding to the peak frequency of the incident wave spectrum. The first four stations are in the upslope and constant shallow depth region where the nonlinear shoaling and harmonic generation take place. The remaining three stations

are in the downslope region and a substantial high-frequency energy is known to be present in the wave-field due to harmonic decomposition. This can be observed by simply comparing the number of zero-crossings at station 2 and station 7. In the computations two components were used with $k_1 = k_p$ and $k_2 = \pi k_p$. Here, k_p denotes the wave-number corresponding to the peak period $T_p = 2$ seconds. The initial condition used was the unperturbed state; that is, both the surface displacement and velocity field were set to zero throughout the computational domain. Time histories of the measured surface displacement at station 1, which was located at the toe of the trapezoidal bar, and the corresponding surface velocity were used as the seaward boundary conditions. At the outgoing boundary the Sommerfeld type radiation boundary condition was implemented. After nearly 10 wave periods elapsed, the wave field established itself fully in the entire numerical domain, allowing comparisons at all the stations. Due to space limitations, the comparisons are given only for five wave periods. Much longer simulations were carried out without any deterioration in agreement with the measurements. The comparisons show clearly that overall the two-component model performs quite well in representing this broad-banded nonlinear wave field. As might be expected, numerical tests with three components brought no sensible improvements.

8. Concluding remarks

A set of fully dispersive weakly nonlinear wave equations has been derived by specifying the vertical dependence of the velocity field in accordance with the solution of Laplace's equation. The Galerkin weak formulation, which is known to be akin to the variational formulations, is employed for solvability. In their most general forms the resulting equations can model the propagation of weakly nonlinear, broad-banded wave fields over arbitrary depths. If the wave-field is narrow banded, the single-component forms of the equations, which require no more computational effort than the Boussinesq equations do, may be used conveniently. As there is no inherit depth restriction on the validity range of these equations they can model the combined effects of nonlinear refraction–diffraction over arbitrary depths, thus closing a long remained gap between nonlinear shallow and deep water waves.

The second author was supported by a grant from the Kajima Foundation of Japan and subsequently from TIT during his stay at TIT. The authors thank Professor J. A. Battjes for his permission to use the experimental data, Mrs E. Tsukamoto for typing the manuscript, and a graduate student O. Ono for helping with the figures. The paper has benefited considerably from the extensive comments of an anonymous reviewer.

Appendix

The following is an excerpt from Beji (1997).

Using the irrotationality conditions, (2.4), it is a straightforward matter to cast the Euler equations, (2.2) and (2.3), into the following forms:

$$\frac{\partial \boldsymbol{u}}{\partial t} + \tfrac{1}{2}\nabla(\boldsymbol{u}\cdot\boldsymbol{u} + w^2) = -\frac{1}{\rho}\nabla p, \tag{1}$$

$$\frac{\partial w}{\partial t} + \frac{1}{2}\frac{\partial}{\partial z}(\boldsymbol{u}\cdot\boldsymbol{u} + w^2) = -\frac{1}{\rho}\frac{\partial p}{\partial z} - g. \tag{2}$$

Alternatively, these equations may be written down from Bernoulli's equation. We

proceed by integrating the vertical momentum equation from an arbitrary depth z to the free surface η:

$$\int_z^\eta \frac{\partial w}{\partial t}\mathrm{d}z + \tfrac{1}{2}(\boldsymbol{u}\cdot\boldsymbol{u}+w^2)\Big|_z^\eta = -\left(\frac{1}{\rho}p+gz\right)\Big|_z^\eta. \tag{3}$$

The dynamic boundary condition, equation (2.5), requires $p(\eta)=0$ so that, from (3), the pressure at an arbitrary depth z is

$$\frac{1}{\rho}p = g(\eta-z) + \int_z^\eta \frac{\partial w}{\partial t}\mathrm{d}z + \tfrac{1}{2}\left[(\boldsymbol{u}_s\cdot\boldsymbol{u}_s+w_s^2)-(\boldsymbol{u}\cdot\boldsymbol{u}+w^2)\right], \tag{4}$$

where the variables evaluated at the free surface $z=\eta$ are denoted as $\boldsymbol{u}_s$, w_s while the variables at an arbitrary depth are left as before. Substitute (4) into (1) to obtain the following alternative form of the equation of motion:

$$\frac{\partial \boldsymbol{u}}{\partial t} + \nabla\left[g\eta + \int_z^\eta \frac{\partial w}{\partial t}\mathrm{d}z + \tfrac{1}{2}(\boldsymbol{u}_s\cdot\boldsymbol{u}_s+w_s^2)\right] = 0, \tag{5}$$

which is *exact* for an irrotational inviscid free surface flow.

References

Beji, S. 1995 Note on a nonlinearity parameter of surface waves. *Coastal Engng* **25**, 81–85.

Beji, S. 1997 Note on conservation equations for nonlinear surface waves. *Ocean Engng* (Submitted.)

Beji, S. & Battjes, J. A. 1994 Numerical simulation of nonlinear wave propagation over a bar. *Coastal Engng* **23**, 1–16.

Beji, S. & Nadaoka, K. 1997 A time-dependent nonlinear mild-slope equation for water waves. *Proc. R. Soc. Lond.* A **453**, 318–332. (Following paper.)

Berkhoff, J. C. W. 1972 Computation of combined refraction-diffraction. In *Proc. 13th Int. Conf. on Coastal Engng*, vol.1, pp. 471–490.

Fenton, J. D. & Rienecker, M. M. 1980 Accurate numerical solutions for nonlinear waves. In *Proc. 17th Int. Conf. on Coastal Engng*, vol. 1, pp. 50–69.

Keller, H. B. 1974 Accurate difference methods for nonlinear two-point boundary value problems. *SIAM J. Num. Analys.* **11**, 305–320.

Kirby, J. T. 1986 A general wave equation for waves over rippled beds. *J. Fluid Mech.* **162**, 171–186.

Madsen, P. A., Murray, R. & Sørensen, O. R. 1991 A new form of the Boussinesq equations with improved linear dispersion characteristics. *Coastal Engng* **15**, 371–388.

Mei, C. C. 1983 *The applied dynamics of ocean surface waves*, p. 740. New York: Wiley.

Miles, J. 1985 Surface waves in basins of variable depth. *J. Fluid Mech.* **152**, 379–389.

Nwogu, O. 1993 Alternative form of Boussinesq equations for near-shore wave propagation. *J. Waterway Port Coastal Ocean Engng* **119-6**, 618-638.

Phillips, O. M. 1960 On the dynamics of unsteady gravity waves of finite amplitude. Part 1. The elementary interactions. *J. Fluid Mech.* **9**, 193–217.

Porter, D. & Staziker, D. J. 1995 Extensions of the mild-slope equation. *J. Fluid Mech.* **300**, 367–382.

Smith, R. & Sprinks, T. 1975 Scattering of surface waves by a conical island. *J. Fluid Mech.* **72**, 373–384.

Witting, J. M. 1984 A unified model for the evolution of nonlinear water waves. *J. Comp. Phys.* **56**, 203–236.

Received 24 October 1995; revised 1 April 1996 and 24 June 1996; accepted 9 July 1996